ACS OMEGA

http://pubs.acs.org/journal/acsodf

Article

Development of a Reduced Chemical Reaction Mechanism for *n*-Pentanol Based on Combined Reduction Methods and Genetic Algorithm

Songfeng Li, Chunhua Zhang,* Zheng Jing, Yangyang Li, Peng Yin, Panpan Cai, and An Lu

Cite This: *ACS Omega* 2021, 6, 6448−6459

Read Online

ACCESS | Metrics & More | Article Recommendations

ABSTRACT: To gradually reduce the demand for fossil energy and accelerate energy transformation, alcohol fuels are being vigorously developed and utilized in the world. *n*-Pentanol as a common alcohol fuel has attracted increasing attention in recent years owing to its many advantages. In this study, a reduced mechanism of *n*-pentanol containing 148 species and 575 reactions was established based on combined reduction methods including the direct relationship graph with error propagation, reaction pathway analysis, rate of production analysis, and temperature sensitivity analysis methods. Then, the reaction rate parameters were optimized using the nondominated sorting genetic algorithm II. A verification experiment for the oxidation of *n*-pentanol was conducted in a jet-stirred reactor (JSR) with gas chromatography-mass spectrometry. The main species mole fractions were quantitatively analyzed in the temperature range 700−1100 K, equivalence ratios of 0.5−2.0, and a pressure of 1 atm. Extensive validations were performed over wide experimental conditions by comparing the experimental data of the ignition delay time, species concentration profiles in the JSR, and laminar flame speed. It was found that the predicted values were in good agreement with the experimental values. Therefore, the reduced mechanism developed in this study can accurately predict the experimental results, which is capable of reasonably applying to the simulation of combustion behaviors of *n*-pentanol in internal combustion engines.

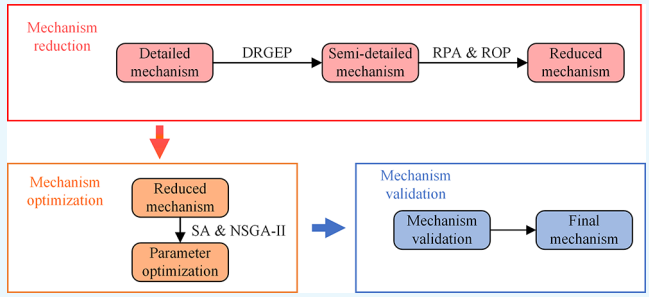

1. INTRODUCTION

Since the energy crisis and environmental pollution have been severe problems all over the world, it will be difficult for the conventional fossil energy to meet the stricter emission and higher fuel economy regulations in the future. To gradually reduce the demand for fossil energy and accelerate energy transformation, biomass fuels are being vigorously developed as a promising alternative energy. Alcohol fuel is a common biomass fuel and belongs to clean and renewable energy. It has a wide source, strong explosion resistance, and low combustion temperature, which is conducive to reducing the emission of NO_x. Therefore, alcohol fuel plays an important role in alternative fuels and emission control of automobile exhaust. Even though alcohol fuel has great advantages, it also faces challenges such as poor ignition property and relatively low energy density.[1] Hence, it is necessary to develop a chemical reaction mechanism and perform an experimental research on this kind of fuel.

At present, ethanol is the most widely produced biofuel.[2] The combustion characteristics and chemical kinetic mechanism of ethanol have been widely studied due to its ease of manufacture and environmental friendliness.[3−8] In addition to reducing greenhouse gas emissions, the use of ethanol can also improve the efficiency of spark ignition engines because of its higher antiknock property and higher laminar burning velocity.[3] Compared with ethanol, butanol and pentanol are also promising biofuels, which have the advantages of higher energy density, lower water solubility, easier storage and transportation, better mixing with fossil fuels, and wide applicability to traditional engines.[9] For this reason, the research on the chemical reaction mechanism of butanol and pentanol has attracted great attention.

Dagaut et al.[10] studied the oxidation of *n*-butanol in a jet-stirred reactor (JSR) using gas chromatography (GC) and developed a novel detailed chemical kinetic mechanism for *n*-butanol oxidation. This mechanism well predicts the concentration of major species under different experimental conditions. Sarathy et al.[11] improved the detailed chemical kinetic mechanism derived by Dagaut et al.,[10] and the

Received: January 9, 2021
Accepted: February 18, 2021
Published: February 26, 2021

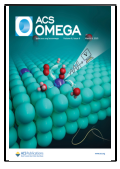

https://dx.doi.org/10.1021/acsomega.1c00147
ACS Omega 2021, 6, 6448−6459

proposed mechanism shows good qualitative agreement with the various experimental data of species concentration profiles in the JSR, laminar flame speed obtained in an *n*-butanol premixed laminar flame, and species concentration profiles for *n*-butanol in an opposed-flow diffusion flame. Harper et al.[12] developed a detailed reaction mechanism for *n*-butanol with 263 species and 3381 reactions by a reaction mechanism generator (RMG). The mechanism was validated by comparing the experimental data, including JSR mole fraction profiles, opposed-flow diffusion flame mole fraction profiles, autoignition delay times, doped methane diffusion flame mole fraction profiles, and newly obtained *n*-butanol pyrolysis experimental results. Zhang et al.[13] measured the ignition delay times of *n*-butanol/oxygen diluted with argon behind reflected shock waves and developed a modified kinetic model for the oxidation of *n*-butanol at high temperature. That model was validated against the measured data and JSR data obtained from the literature.

Heufer et al.[14] presented a detailed kinetic model for *n*-pentanol based on the modeling rules previously presented for *n*-butanol.[11] The proposed model was validated against ignition delay time data, speciation data from JSR, and laminar flame speed. The simulation results showed good agreement with the experiments. Togbé et al.[15] studied the oxidation of 1-pentanol in a JSR and measured the laminar flame speeds of 1-pentanol−air premixed laminar flame at 1 atm and 423 K for equivalence ratios of 0.7−1.4. They proposed a detailed chemical kinetic reaction mechanism and verified with the metrical experimental data. Wang et al.[16] investigated the flow reactor pyrolysis and laminar premixed flames of *n*-pentanol and developed a detailed *n*-pentanol kinetic model consisting of 314 species and 1602 reactions. The proposed model was validated on the experimental results of pyrolysis and flame. Dayma,[17] Tsujimura,[18] and Sarathy[19] et al. developed detailed chemical reaction kinetics models for isopentanol (3-methyl-1-butanol). The first two models were validated with experimental data of concentration profiles of stable species in JSR and ignition delay data in a shock tube (ST) and a rapid compression machine (RCM), respectively. While the last model was validated with the experimental data for iso-pentanol in ST, RCM, JSR, and counter flow diffusion flame. Li et al.[20] studied the laminar combustion characteristics and chemical kinetics of four pentanol isomer−air mixtures and developed a model for four pentanol isomers and validated against the data of laminar flame speed as well as ignition delay times.

For practical applications, the chemical kinetic mechanism coupled with the computational fluid dynamics (CFD) has been an increasingly common method in internal combustion engine research.[21] However, direct coupling of the detailed mechanism with the multidimensional CFD model is unrealistic because the detailed chemical kinetic mechanism is typically complex. Therefore, it is necessary to reduce the chemical kinetic mechanisms to reduce the computation cost while maintaining the essential dynamic features of the kinetic model. Some studies focused on mechanism reduction using different reduction methods. Feng et al.[22] developed a reduced mechanism for *n*-butanol combustion using a series of combined reduction methods. The reduced mechanism was validated against ST and JSR data. Díaz-González et al.[23] developed a reduced chemical mechanism of *n*-butanol in air. The predicted results of the mechanism showed an excellent agreement against the experimental data of laminar flame speed, ignition delay time, and JSR. They confirmed that the reduced mechanism could be used instead of detailed mechanisms, especially considering the current computational capability to simulate the practical combustion systems. However, a few studies have focused on the reduced mechanism for *n*-pentanol combustion. Liu et al.[24] developed a combined reduced kinetic mechanism for primary reference fuel-alcohols containing methanol, ethanol, propanol, etc. The reduced mechanism was validated with the experimental data of ignition delay time, laminar flame speeds, and mole fraction profiles of species and was used for the three-dimensional modeling studies by coupling with the toluene−polycyclic aromatic hydrocarbons submechanism. Chang et al.[25] developed a skeletal oxidation mechanism for *n*-pentanol. The oxidation mechanism was established based on the decoupling methodology, and then the rate constants of related reactions were optimized in the mechanism. The final mechanism was determined by comparing the uncertainty of optimal prediction with the available experimental data. The optimized mechanism was validated against measurements in ST, RCM, JSR, and premixed laminar flame.

The mechanism optimization by amending the reaction rate constant is an important step in the study on mechanism reduction. The traditional parameter optimization process is based on the manual iteration of sensitivity analysis (SA) and path analysis, which is a time-consuming process and greatly depends on the handler's experiences.

In the present work, a reduced chemical kinetic mechanism for *n*-pentanol was developed with combined reduction methods including the direct relationship graph with error propagation (DREGP), reaction pathway analysis (RPA), rate of production (ROP) analysis, and temperature sensitivity analysis (SA) methods. Moreover, the kinetic parameters of the related reactions were optimized to guarantee the computational accuracy of the simplified mechanism by the nondominated sorting genetic algorithm II (NSGA-II). The applicability of the reduced mechanism covers the oxidation process of *n*-pentanol at medium and low temperatures and major species concentration predictions. In addition, the experiments were performed in a JSR to study the oxidation of *n*-pentanol at a pressure of 1 atm and a range of equivalence ratios from 0.5 to 2.0 and temperatures of 700−1150 K. The reduced mechanism was validated with the experimental data of species profiles in JSR, ignition delay times, and laminar flame speeds.

2. MECHANISM REDUCTION

A detailed chemical kinetic mechanism could fully describe the combustion process of *n*-pentanol. However, it is impractical to be used for multidimensional numerical computation because of the excessive time consumption of the larger reaction mechanism. Therefore, establishing a reduced medium- to low-temperature oxidation mechanism for *n*-pentanol is necessary. To obtain an effective reduced mechanism, the closed homogeneous batch reactor in CHEMKIN package was used to simulate the reaction process of *n*-pentanol. Meanwhile, the species concentrations in JSR and laminar flame speed in a heated spherical bomb were computed by a perfectly stirred reactor (PSR) and a premixed laminar flame-speed calculation reactor, respectively. In this study, the detailed mechanism of *n*-pentanol developed by Heufer et al.[14] was chosen as the base mechanism, which was composed of 599 species and 3010 reactions. This mechanism was verified by a wide range of

https://dx.doi.org/10.1021/acsomega.1c00147
ACS Omega 2021, 6, 6448−6459

experimental data, according to the predicted results. The reduced mechanism for *n*-pentanol was developed from the base mechanism with the combination method. The DRGEP method was used for the preliminary reduction to remove the unimportant components and primitive reactions. The reaction path analysis and the rate of production analysis were utilized for lumping isomers to further reduce the size of the mechanism. Then, the relatively sensitive reactions to fuel combustion were determined through the temperature sensitivity analysis method and the rate constants of the reactions in the obtained mechanism were optimized with the genetic algorithm, to reproduce the major species concentrations in the JSR, the ignition delay times, and the laminar flame speeds.

2.1. Direct Relationship Graph with Error Propagation Method. To eliminate unimportant species and reactions in the detailed mechanism, a preliminary reduction with the DRGEP method was performed at an initial pressure of 1 atm, a temperature range of 700−1100 K, and an equivalence ratio of 0.1−2.0. The main intermediate species such as CH_4, C_3H_6, CH_3CHO, C_3H_7CHO, C_2H_4, and C_4H_9CHO were selected as the target components, along with the fuel $C_5H_{11}OH$, oxide O_2, the reaction product CO_2 and H_2O, which are essential species in the simplification process. Based on the closed-type homogeneous reactor model, the semidetailed mechanisms of different components and reactions were obtained by the simplified calculation with different error thresholds from small to large. Two semidetailed mechanisms (#1 182 species, 1006 reactions; #2 235 species, 1284 reactions) were obtained. The ignition delay times predicted by the two semidetailed mechanisms and the detailed mechanism are illustrated in Figure 1. Figure 1a shows the predicted results at an equivalence ratio of 1.0 and diverse pressure and temperature. It can be seen that both the semidetailed mechanisms can accurately predict the ignition delay times in a high temperature range at all pressures. Figure 1b shows the predicted results at a pressure of 10 atm and diverse equivalence ratio and temperature. It can be seen that the ignition delay times decrease with the increase of the equivalence ratio. This can be attributed to a higher mixture concentration, which accelerates the oxidation reactions of the fuel and thus reduces the ignition preparation time. In general, in a low temperature range, the semidetailed mechanism containing 235 species and 1284 reactions fits better with the detailed mechanism and slightly overpredicts the ignition delay times. Thus, the semidetailed mechanism with 235 species and 1284 reactions was selected for further reduction.

2.2. Reaction Path Analysis and Rate of Production Analysis Methods. The isomers of intermediate species should be lumped for further reducing the size of the semidetailed mechanism. To determine the respective production fraction of isomers during the oxidation reaction process and define the representative isomers of intermediate species, the RPA and ROP analysis were performed at an initial pressure of 10 atm, an equivalence ratio of 1.0, and initial temperatures of 800 and 1100 K. The major reaction pathways for *n*-pentanol combustion at 20% fuel consumption are depicted in Figure 2. It can be found that the main consumption reactions of *n*-pentanol are H-abstraction reactions by hydroxyl (OH) and hydroperoxyl (HO_2) radicals, which produce the following isomers: $C_5H_{10}OH$-11, $C_5H_{10}OH$-12, $C_5H_{10}OH$-13, $C_5H_{10}OH$-14, $C_5H_{10}OH$-15, and $C_5H_{11}O$. As shown, about 50% of *n*-pentanol was dehydrogenated to form $C_5H_{10}OH$-11, while a little fuel reacts with OH and HO_2 to form $C_5H_{11}O$ at 800 K. In addition, 20.7 and 11.8% of *n*-pentanol were dehydrogenated to form $C_5H_{10}OH$-14 and $C_5H_{10}OH$-13, respectively, which was higher than other isomers. Similar to the pathways at low temperature, most of *n*-pentanol was consumed to form $C_5H_{10}OH$-11 and only a fraction of the fuel was converted to $C_5H_{11}O$ at 1100 K. $C_5H_{10}OH$-14 and $C_5H_{10}OH$-13 also have a higher yield than any other isomer except $C_5H_{10}OH$-11.

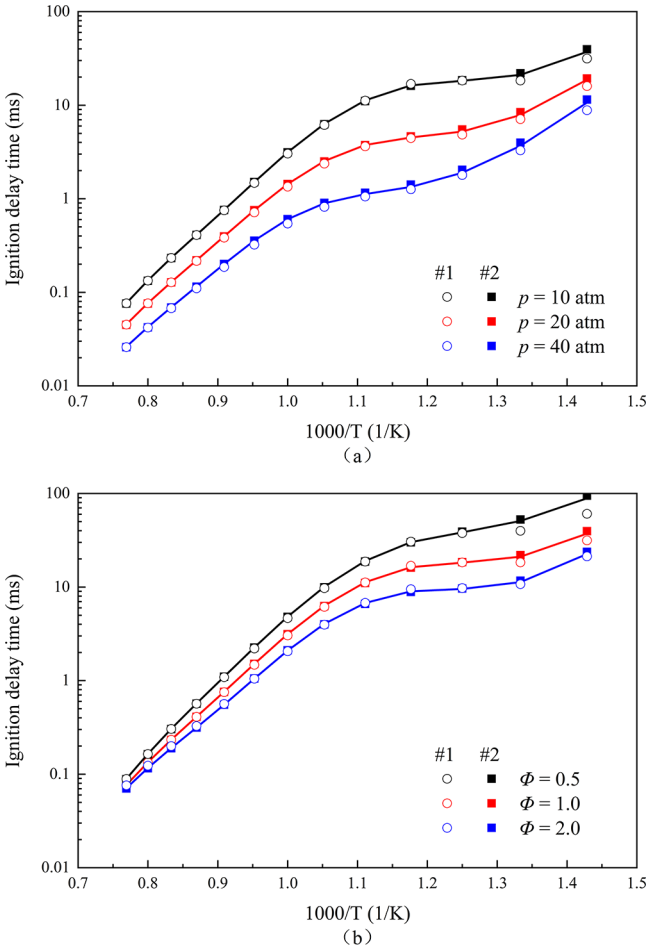

Figure 1. Comparison of the predicted ignition delay times by the two semidetailed mechanisms and the detailed mechanism at a (a) pressure of 10−40 atm and (b) equivalence ratio of 0.5−2.0 (lines are the predictions of the detailed mechanism, and symbols are the predictions of two semidetailed mechanisms: #1 182 species, 1006 reactions; #2 235 species, 1284 reactions).

Figure 3 illustrates the total rate of production for each isomer of $C_5H_{10}OH$ at a pressure of 10 atm, an equivalence ratio of 1.0, and temperatures of 800 and 1100 K. The total rate of production represents the sum of the rates of all reactions that produce the corresponding isomers. It can be observed that the rate of production of $C_5H_{10}OH$-11 was the highest, followed by $C_5H_{10}OH$-14 and $C_5H_{10}OH$-13 at 800 K. Similarly, the formation rate of $C_5H_{10}OH$-11 was the highest at 1100 K though the proportion was reduced by 17% compared to the low temperature, while the formation rate of $C_5H_{11}O$ was the lowest. The formation rates of $C_5H_{10}OH$-14 and $C_5H_{10}OH$-13 were still higher than those of other isomers except $C_5H_{10}OH$-11. This can be attributed to the different C−H bond energies of *n*-pentanol, and so the C−H bond

https://dx.doi.org/10.1021/acsomega.1c00147
ACS Omega 2021, 6, 6448−6459

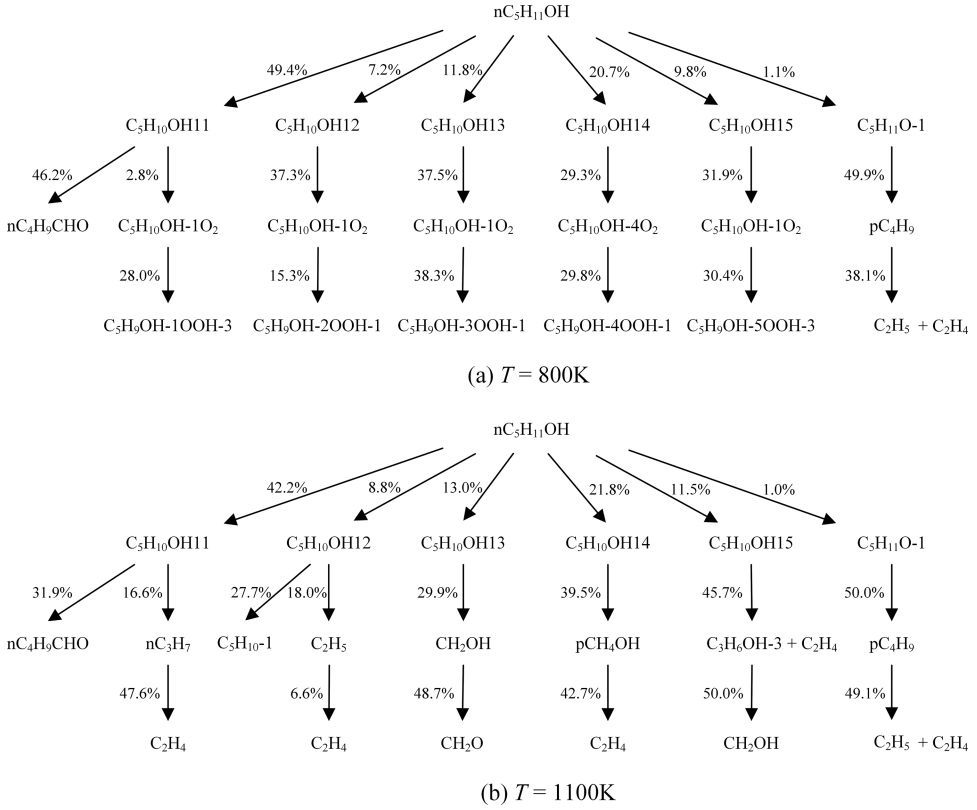

Figure 2. Major reaction pathways for *n*-pentanol combustion.

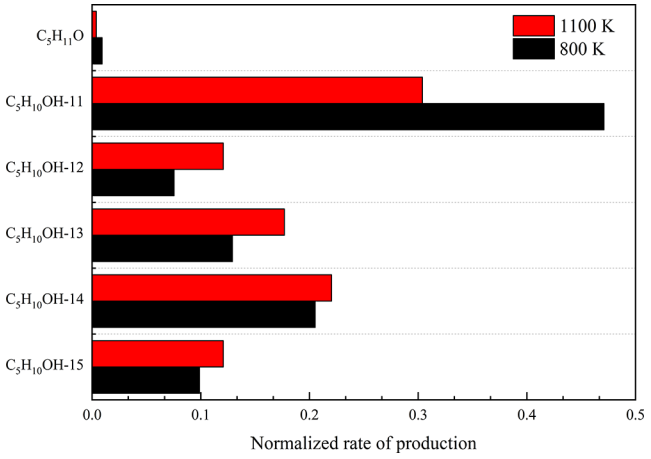

Figure 3. Total rate of production for each isomer of *n*-pentanol.

breaks in a different order. The C−H bond energies can be sorted according to priority as follows:[14] C_α−H < C_s−H < C_γ−H < C_β−H < C_p−H < O−H. The smaller the bond energy, the more likely it is to break. Therefore, H atoms at the α carbon and s carbon are the easiest to be captured and the formation rates of $C_5H_{10}OH$-11 and $C_5H_{10}OH$-14 are higher than other isomers.

The above analysis shows that the relatively important components of $C_5H_{10}OH$ isomers are $C_5H_{10}OH$-11, $C_5H_{10}OH$-13, and $C_5H_{10}OH$-14 radicals. To further simplify the semidetailed mechanism, the species and reactions related to $C_5H_{10}OH$-12, $C_5H_{10}OH$-15, and $C_5H_{11}O$ radicals were removed and only the species and reactions related to $C_5H_{10}OH$-11, $C_5H_{10}OH$-13, and $C_5H_{10}OH$-14 radicals were reserved. Finally, a simplified mechanism of *n*-pentanol containing 148 species and 575 reactions was obtained.

2.3. Optimization of Kinetic Parameters. After the construction of the new reduced mechanism, the kinetic parameters need to be optimized to meet the accuracy requirements under various working conditions and make the reduced mechanism better fit the detailed mechanism. However, each reaction in the simplified mechanism of *n*-pentanol has a greater or lesser effect on the ignition delay time. Therefore, a temperature sensitivity analysis was performed at a pressure of 10 atm, an equivalence ratio of 0.5−2.0, and initial temperatures of 800 and 1100 K to evaluate the contribution of each reaction to the ignition delay time. The temperature sensitivity coefficients of each reaction are calculated by the following equation

$$S = \frac{\log \tau_+ - \log \tau_-}{\log 2 - \log 0.5} \quad (1)$$

where S represents the temperature sensitivity coefficient and τ_+ and τ_- are the ignition delay time predicted by the obtained reduced mechanism with the reaction rate constant multiplied by a factor of 2 and 0.5, respectively. A positive sensitivity indicates that the reaction promotes the overall reactivity, while a low reactivity is indicated by a negative sensitivity. The temperature sensitivity coefficient for *n*-pentanol combustion under various conditions is shown in Figure 4. It can be found that the effects of each reaction on the ignition delay time are significantly discrepant at different temperatures. Figure 4a shows the normalized temperature sensitivity coefficient of the most active reactions at 800 K. Direct fuel consumption reactions R12 and R13 are the two most active reaction pathways, which have opposite sensitivity coefficients. This

https://dx.doi.org/10.1021/acsomega.1c00147
ACS Omega 2021, 6, 6448−6459

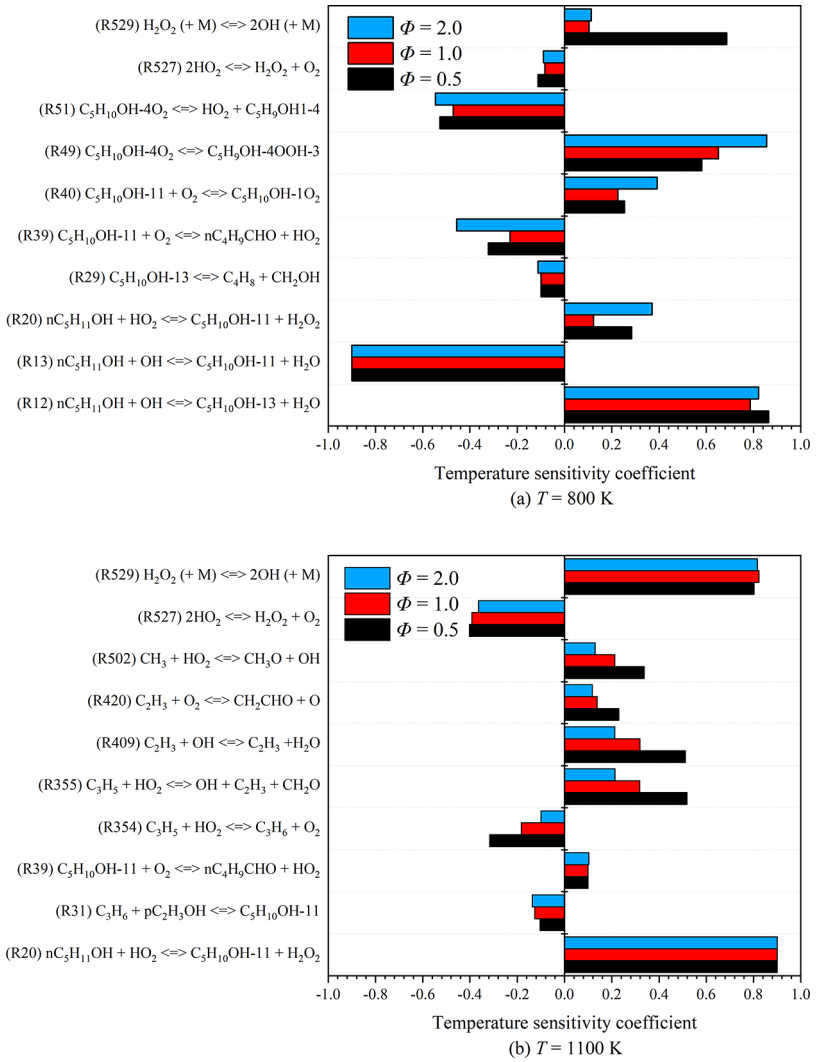

Figure 4. Temperature sensitivity coefficient for *n*-pentanol combustion at T = 800 K (a) and 1100 K (b).

indicates that there is a direct competitive relationship between R12 and R13, which reduces the reactivity of oxidation reaction at low temperatures. The next reactions that have the most impact on the temperature are reactions R49 and R51, resulting in a direct removal of the radical $C_5H_{10}OH{-}4O_2$. As shown in Figure 4b, the reactions that demonstrate high temperature sensitivity coefficients at 1100 K are quite different from those at low temperatures. The most active reaction pathway is $nC_5H_{11}OH + HO_2 \Leftrightarrow C_5H_{10}OH\text{-}11 + H_2O_2$ (R20), a fuel consumption reaction with hydroperoxy radical HO_2 instead of hydroxyl radical OH. The next is H_2O_2 (+M) ⇔ 2OH (+M) (R529), which promotes the fuel oxidation reaction and shortens the ignition delay time. Similar conclusions can be found from a previous study,[26] which concludes that the ignition delay times of primary alcohols are observably sensitive to the initial H-abstraction reaction with HO_2 radicals. The H-abstraction reaction traps the relatively active HO_2 radicals into the stable H_2O_2 molecules and H_2O_2 fragments to generate OH radicals as the temperature increases, restoring the oxidation capacity. Thus, R20 and R529 play an important role in this stage. In contrast, the reactions with higher sensitivity coefficients at low temperatures, such as R12 and R13, are less active at high temperatures. This indicates that the low-temperature kinetics promotes the reaction in its initial stage, while the high-temperature kinetics dominates the reaction. Therefore, modifying the rate constants of one specific reaction with high sensitivity coefficients can affect the ignition delay time at certain initial temperature regions and then improve the performance of the mechanism.

The kinetic parameter optimization was carried out by modifying the reaction rate constants for the key reactions identified in the above analysis. The reaction rate constants are defined as Arrhenius equation

$$k = A \exp\left(-\frac{E}{RT}\right) \tag{2}$$

where A is the pre-exponential factor and E is the activation energy of each reaction. R represents the universal gas constant, and T represents the catalyst surface temperature. Accordingly, the reaction rate is dependent on the pre-exponential factor A and the activation energy E. Therefore, the key to parameter optimization is to improve the pre-exponential factor and the activation energy by comparing them with the experimental data. Generally, the parameter optimization process is to change the parameter value of the mechanism so that the objective function reaches the maximum or minimum value. The objective function describes

https://dx.doi.org/10.1021/acsomega.1c00147
ACS Omega 2021, 6, 6448−6459

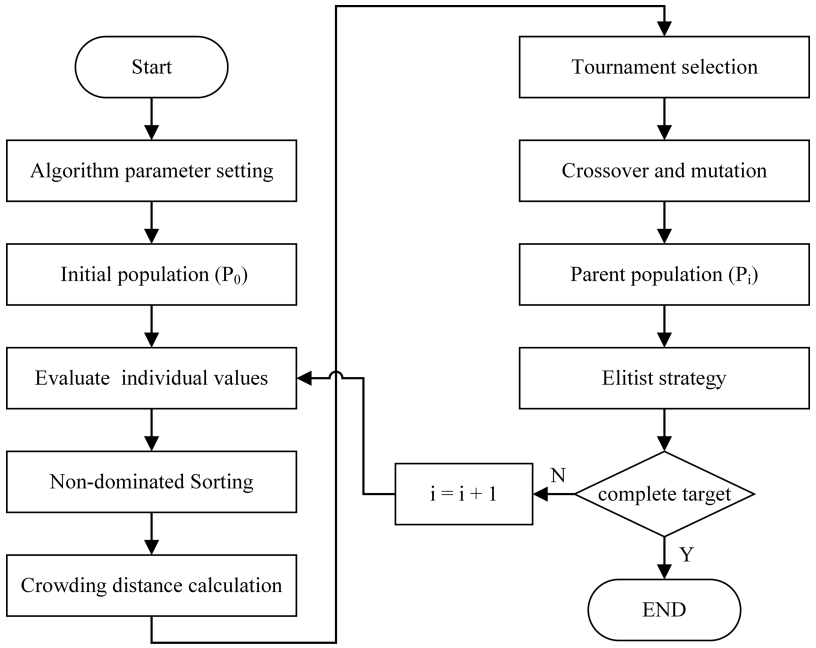

Figure 5. Flowchart of the NSGA-II algorithm.

Table 1. Optimization of Kinetics Parameters

reaction number	reaction	original A	modified A
R12	$nC_5H_{11}OH + OH \Leftrightarrow C_5H_{10}OH\text{-}13 + H_2O$	1.141×10^3	2.8×10^3
R20	$nC_5H_{11}OH + HO_2 \Leftrightarrow C_5H_{10}OH\text{-}11 + H_2O_2$	3.50×10^{-5}	1.12×10^{-4}
R51	$C_5H_{10}OH\text{-}4O_2 \Leftrightarrow HO_2 + C_5H_9OH1\text{-}4$	4.31×10^{36}	8.62×10^{36}

a theoretically achievable goal, which plays a significantly important role in the parameter optimization process. In this work, the objective function is defined as the residual sum of squares between experimental and simulation values.

$$f_i = \frac{\sum_{i=1}^{n} (\tau_{i,d} - \tau_{i,r})^2}{n} \quad (3)$$

where $\tau_{i,d}$ and $\tau_{i,r}$ are the ignition delay times predicted by detailed and reduced mechanisms, respectively. By solving the objective function, the reaction rate equation and optimal reaction rate constants can be determined to achieve the best fitting between model simulation and experimental measurement under each test condition.

In this work, a multiobjective genetic algorithm, NSGA-II, was used to optimize the reaction rate constants automatically for each element reaction. NSGA-II is the optimization of the traditional genetic algorithm, which reflected in the following three aspects: First, based on nondominated sorting, all of the individuals in the population are stratified by evaluating the target value, which reduces the computational complexity and improves the solving speed. Second, the elite strategy has been designed in the process of selecting operation. Some inferior individuals are eliminated after the generation of new population and the superior individuals in the parent population are selected to retain for the new population. Last, NSGA-II proposes the definition of the crowding distance operator. The crowding distances between each individual are calculated to avoid excessive concentration of individuals and falling into the local optimal solution. The application of nondominated sorting, elitist strategy, and crowding distance can reduce the computational complexity and retain the Pareto-optimal solution. The steps of NSGA-II algorithm are shown in Figure 5. The NSGA-II algorithm runs with a population size of 50, a generation size of 200, a crossover probability of 0.65, a mutation probability of 0.05, the crossover distribution index of 10, and the mutation distribution index of 10. Considering the sensitivity of each reaction at low and high temperatures, three reactions (R12, R20, and R51) were finally screened. Their reaction rate constants were used as the initial chromosome population to randomly generate initial populations. Then, the ignition delay times of the initial mechanisms were computed using the CHEMKIN package and the results obtained were used for calculating the objective function and crowding distance. The new population was generated through tournament selection, and crossover and mutation and the ignition delay times of the new mechanisms were computed again. All of the individuals in the initial population and new population were combined into a unified population and superior individuals from the unified population were selected by the elitism strategy as the next generation. The optimization process described above is repeated until the target generation is reached and a set of optimized reaction rate constants are obtained. The optimal values of the resulting kinetic parameters are given in Table 1.

3. RESULTS AND DISCUSSION

3.1. Ignition Delay Times. Simulations for predicting the ignition delay times were performed using the constant-volume homogeneous batch reactor module in the CHEMKIN package, and the ignition moment is defined as the time when the temperature increases to 400 K above the T_{in}. The experimental ignition delay time data was measured by Heufer

https://dx.doi.org/10.1021/acsomega.1c00147
ACS Omega 2021, 6, 6448−6459

et al.[27] using a high-pressure ST and in an RCM at a pressure of 9 bar and an equivalence ratio Φ = 1.0. Figure 6 shows the

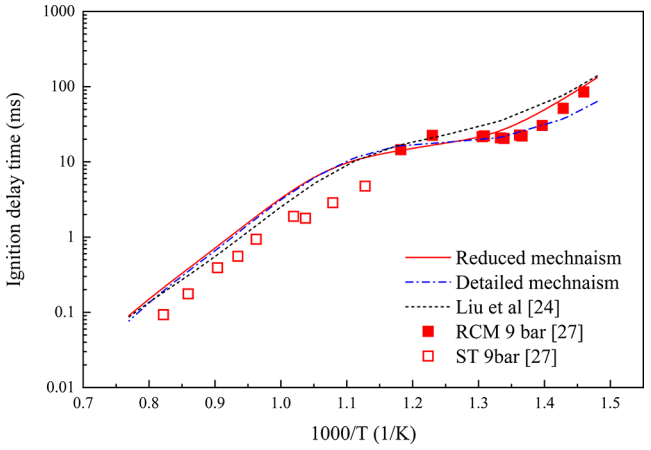

Figure 6. Comparisons of the ignition delay times between the experimental measurement and the mechanism prediction.

comparison of ignition delay times for *n*-pentanol−air mixtures between the reduced mechanism, detailed mechanism, and experimental data. It can be found that the ignition delay times predicted by the reduced mechanism can achieve a good agreement with the prediction of the detailed mechanism, except for the low-temperature stage, which is slightly longer than the simulation values of the detailed mechanism in the low-temperature region. This is because the detailed mechanism of *n*-pentanol contains a large part of the components involved in the low-temperature reaction, which are removed in the reduced mechanism as unimportant components and reactions. So, the prediction results of the reduced mechanism at low temperatures are slightly inaccurate. Compared with the mechanism of Liu et al.,[24] the reduced mechanism presented in this paper performs slightly worse at high temperatures but has a great improvement in a range of low temperatures. Overall, the ignition delay times predicted by the reduced mechanism can achieve a good agreement with the experimental results, which indicates that the reduced mechanism well predicts the ignition characteristics under various conditions.

3.2. Species Concentrations in the JSR. The experiments were performed at a constant mean residence time of 2.0 s, a pressure of 1 atm, and temperature range of 700−1100 K. The equivalence ratio was varied from 0.5 to 2.0, while the fuel initial concentration was fixed at 1000 ppm. Simulations for predicting species concentration in the JSR were performed using the PSR module in the CHEMKIN package. In this paper, the transient solver was used to solve the reaction process with an end time set as 20 s, so that the reaction occurs sufficiently until the species molar fractions no longer change over time for acquiring steady data at each condition. The mole fractions of *n*-pentanol and the main oxidation species were predicted under the same conditions as the experiment to verify the accuracy of the reduced mechanism.

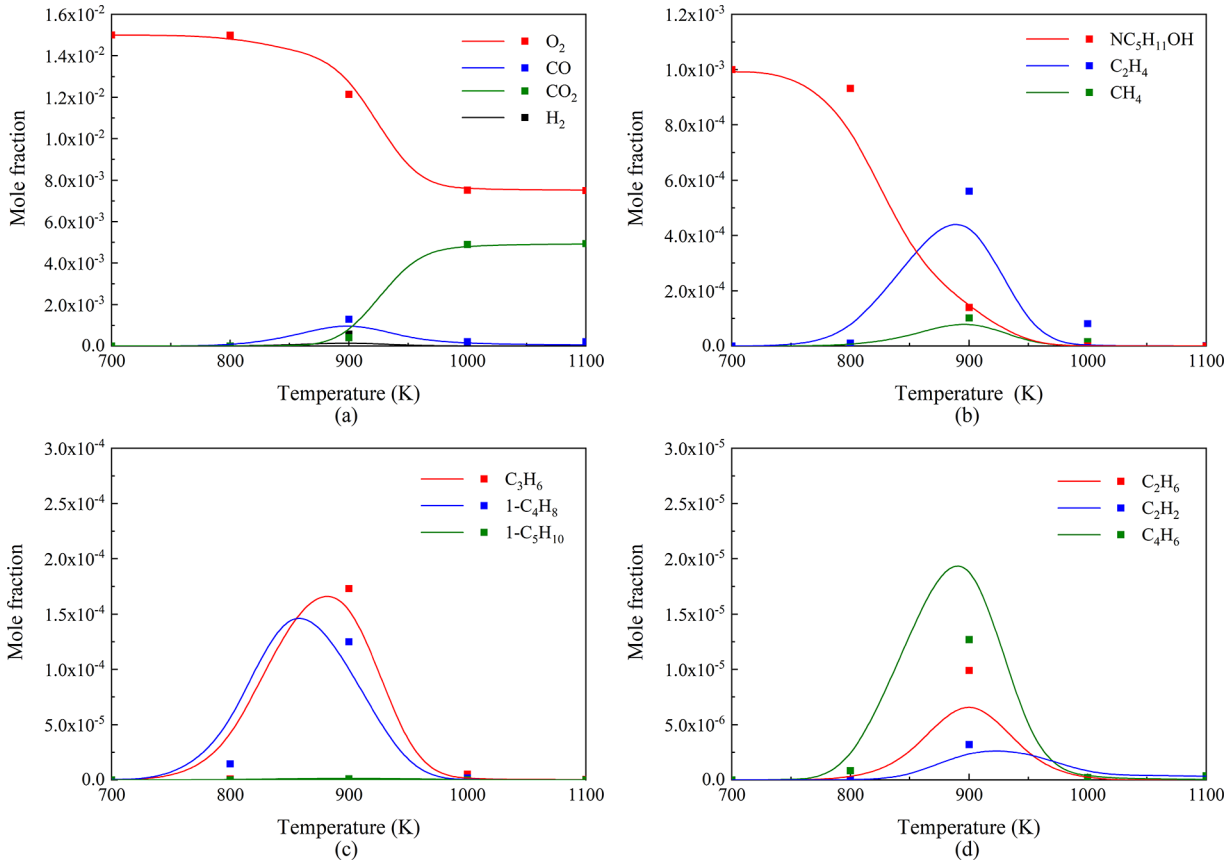

Figure 7. Comparison of the species concentration in the JSR between the experimental measurement and mechanism prediction at an equivalence ratio of 0.5: (a) $O_2/CO/CO_2/H_2$, (b) $NC_5H_{11}OH/C_2H_4/CH_4$, (c) $C_3H_6/1\text{-}C_4H_8/1\text{-}C_5H_{10}$, and (d) $C_2H_6/C_2H_2/C_4H_6$ (lines are the predictions of the reduced mechanism, and symbols are the experimental results).

https://dx.doi.org/10.1021/acsomega.1c00147
ACS Omega 2021, 6, 6448−6459

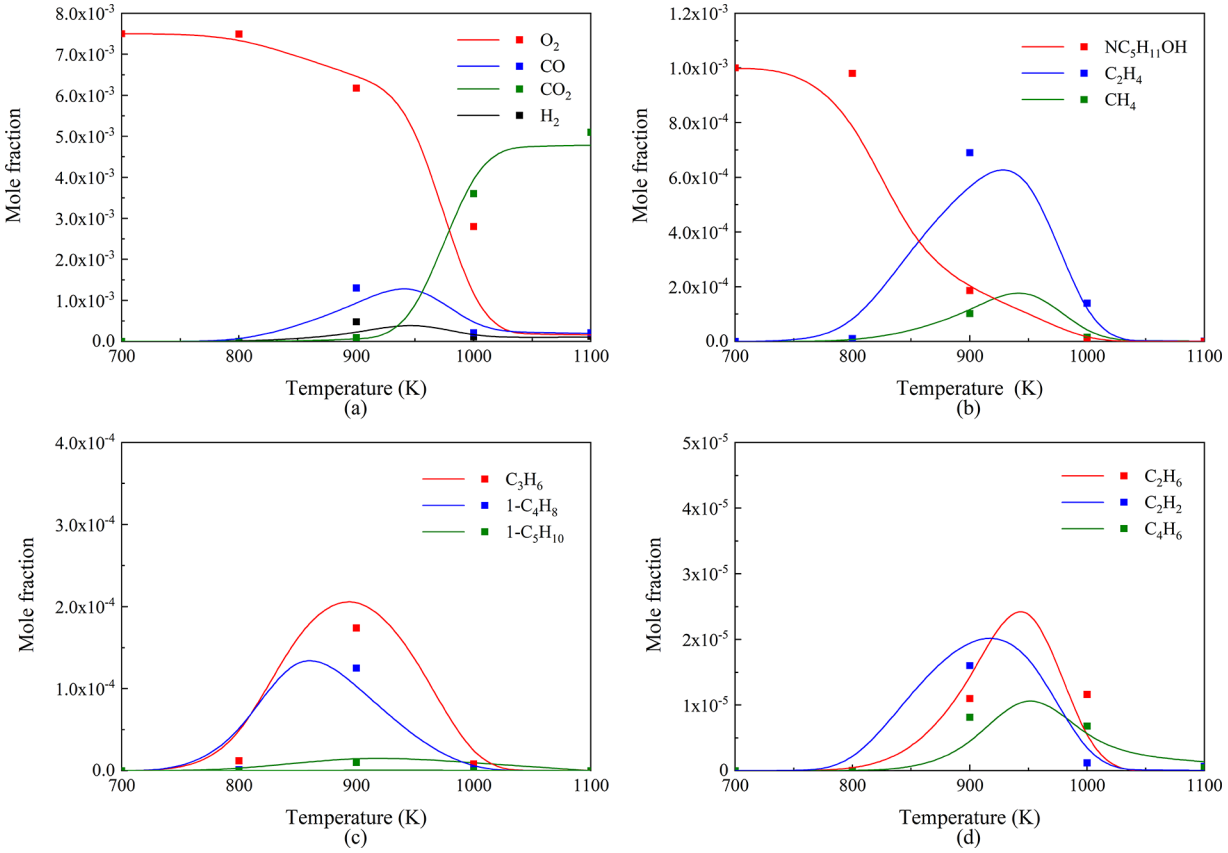

Figure 8. Comparison of the species concentration in the JSR between the experimental measurement and mechanism prediction at an equivalence ratio of 1.0: (a) $O_2/CO/CO_2/H_2$, (b) $NC_5H_{11}OH/C_2H_4/CH_4$, (c) $C_3H_6/1\text{-}C_4H_8/1\text{-}C_5H_{10}$, and (d) $C_2H_6/C_2H_2/C_4H_6$ (lines are the predictions of the reduced mechanism, and symbols are the experimental results).

Figures 7−9 show the comparisons of species concentrations in the JSR between the simulation results predicted by the reduced mechanism and the experimental data at equivalence ratios of 0.5, 1.0, and 2.0, respectively. The mole fractions of the main oxidation species (H_2, CO, CO_2, CH_4, C_2H_6, C_2H_2, C_2H_4, C_3H_6, 1-C_4H_8, 1-C_5H_{10}, and C_4H_6) and the reactants ($nC_5H_{11}OH$ and O_2) were considered in the current validations. Generally, the agreement between the measurements and the predicted results on the reactants and major products is satisfactory. It can be seen that the fuel begins to oxidize at about 800 K, accompanied by rapid depletion of reactants and rapid formation of small species. This is also well reflected in the prediction results of the reduced mechanism. The major small molecule oxidation products, such as CO, CO_2, and H_2, are well predicted by the reduced mechanism around the entire temperature range. However, there are slight discrepancies between the experiments and the predicted results on the macromolecular species (i.e., C_3H_6, C_2H_4, and C_4H_6). This is mainly due to the removal of species and reactions involved in the formation and decomposition of these species, leading to a change in the pathway of the reaction. As can be seen from Figure 2, in the detailed mechanism, 26.7% of $C_5H_{10}OH_{12}$ decomposes to generate C_5H_{10}-1 and OH radical, 45.7% of $C_5H_{10}OH_{15}$ cleaves to C_2H_4 and C_3H_6OH-3, and 50% of $C_5H_{11}O$-1 decomposes to pC_4H_9, which is able to further generate C_2H_4. In the process of lumping isomers, the removal of these intermediate species results in the underprediction of C_5H_{10}-1 and C_2H_4 by the reduced mechanism. In addition, C_4H_6 is mainly generated by the decomposition of C_4H_6OH1-32 and the dehydrogenation of $C_4H_7$1-3 in the detailed mechanism. Meanwhile, C_4H_6 can decompose to C_4H_5 through dehydrogenation reaction, and the reaction flow accounts for 48% of the total reaction flow. After the reduction of the mechanism, the reaction flow has changed. All of the C_4H_6 is generated from C_4H_6OH1-32 pyrolysis and completely dehydrogenates to C_4H_5. The difference in the reaction flow results in the discrepancy between the predicted and experimental values. On the other hand, the DRGEP reductions were carried out on a constant-volume homogeneous batch reactor, which is different from the jet-stirred reactor. This ultimately affects the prediction of the species concentrations in the JSR. Overall, the simulated values for the mole fraction of the main components of the reduced mechanism are in good agreement with the experimental data. This indicates that the reduced mechanism has satisfactory prediction accuracy.

3.3. Laminar Flame Speeds. The laminar flame speed is an effective means to verify the mechanism of combustion dynamics, just like the concentrations of the reactive substances in the JSR and the ignition delay times. Simulations for predicting the laminar flame speed were performed using the premixed laminar flame-speed calculation module in the CHEMKIN package. The experimental laminar flame speeds of *n*-pentanol data were measured by Nativel et al.[28] using a heated spherical bomb over a range of equivalence ratios (0.7−1.5). Figure 10 shows the comparison of laminar flame speeds for *n*-pentanol−air mixtures between the reduced mechanism and experimental data at a pressure of 1 atm and temperature

https://dx.doi.org/10.1021/acsomega.1c00147
ACS Omega 2021, 6, 6448−6459

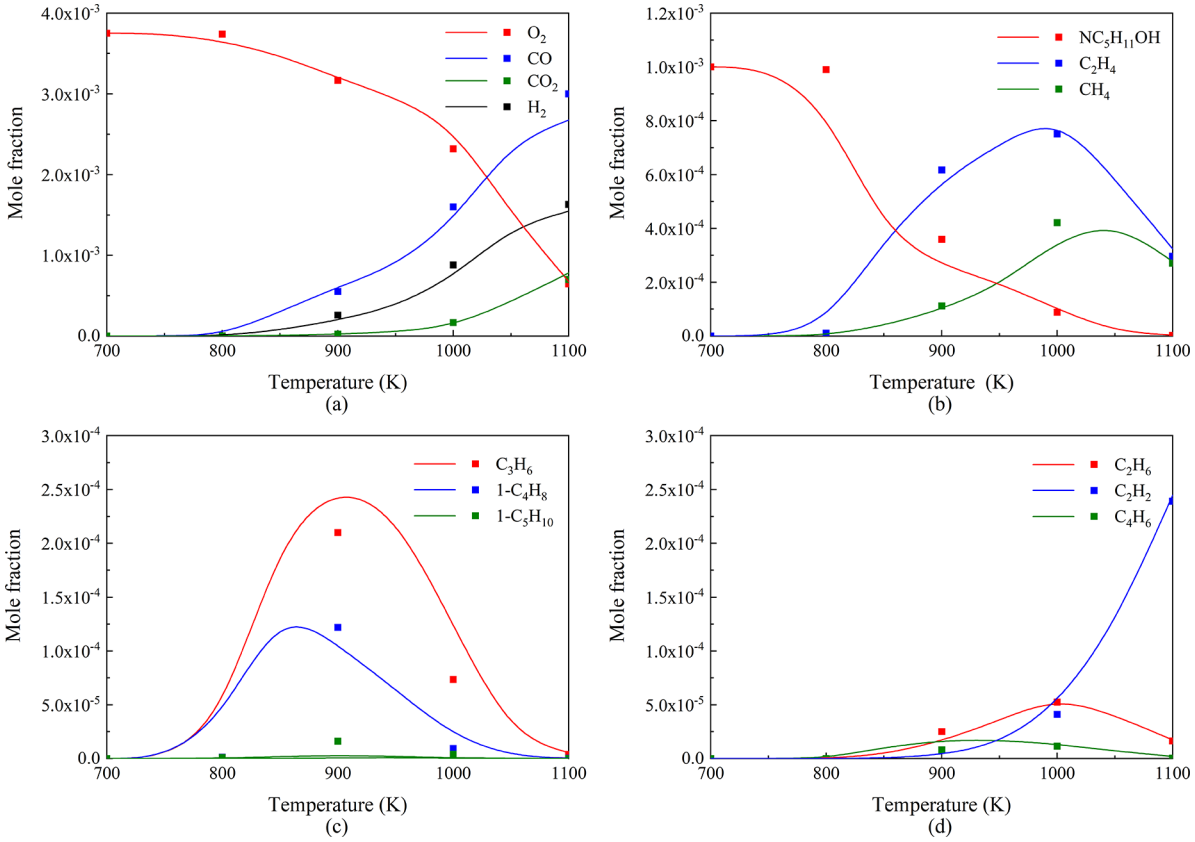

Figure 9. Comparison of the species concentration in the JSR between the experimental measurement and mechanism prediction at an equivalence ratio of 2.0: (a) $O_2/CO/CO_2/H_2$, (b) $NC_5H_{11}OH/C_2H_4/CH_4$, (c) $C_3H_6/1\text{-}C_4H_8/1\text{-}C_5H_{10}$, and (d) $C_2H_6/C_2H_2/C_4H_6$ (lines are the predictions of the reduced mechanism, and symbols are the experimental results).

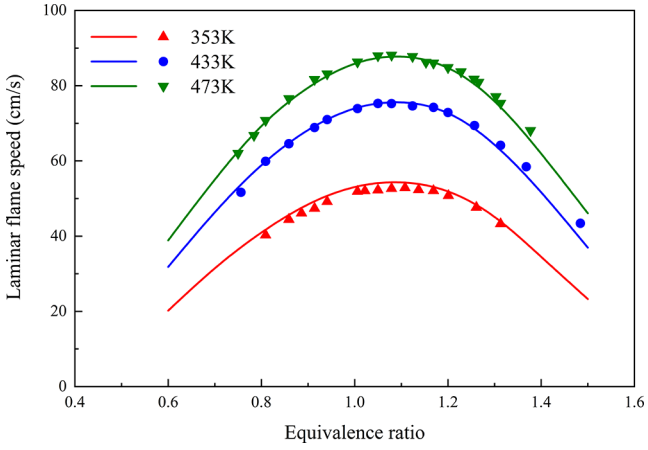

Figure 10. Comparison of the laminar flame speed between the experimental measurement and mechanism prediction (lines are the predictions of the reduced mechanism, and symbols are the experimental results).

in the range of 353−473 K. It can be seen that the reduced mechanism well matches with the experimental data. At all temperatures, the laminar flame speed first increases with increasing equivalence ratio, while the experimental results and prediction results of the laminar flame speed reach a peak at Φ = 1.1. However, the increase of equivalence ratio will decrease the laminar flame speed when the equivalence ratio exceeds 1.1. This is due to the lack of fuel in the thinner mixture, resulting in less heat release, which reduces the laminar flame speed. In thicker mixtures, the lack of oxidants can also lead to worse combustion and lower reaction speed. Moreover, the laminar flame speed increases with the increase of temperature, which is also well reproduced by the reduced mechanism. Overall, although the current mechanism slightly underpredicts those under fuel-rich conditions, the reduced mechanism well predicts the experimental data over a wide range of operating conditions. Therefore, the trends of laminar flame speed are well represented by the reduced *n*-pentanol mechanism with satisfactory accuracy.

4. CONCLUSIONS

In this work, a new reduced chemical kinetic mechanism was developed to capture the oxidation characteristics of *n*-pentanol based on the combined reduction methods including the DREGP, RPA, ROP, and SA methods. Additionally, the kinetic parameters of the related reactions in the reduced mechanism are optimized by NSGA-II to guarantee the computational accuracy of the reduced mechanism. A verification experiment was conducted in the JSR at 1 atm, 700−1100 K, and equivalence ratios between 0.5 and 2.0 to measure the concentrations of major species using gas chromatography-mass spectrometry (GC-MS). In addition, the ignition delay times and laminar flame speeds were also utilized to compare with the calculation of the proposed chemical kinetic mechanism.

The final chemical kinetics mechanism composed of 148 species and 575 reactions has been extensively validated against the ignition delay times, species concentration profiles in the JSR, and laminar flame speeds over a wide range of

https://dx.doi.org/10.1021/acsomega.1c00147
ACS Omega 2021, 6, 6448−6459

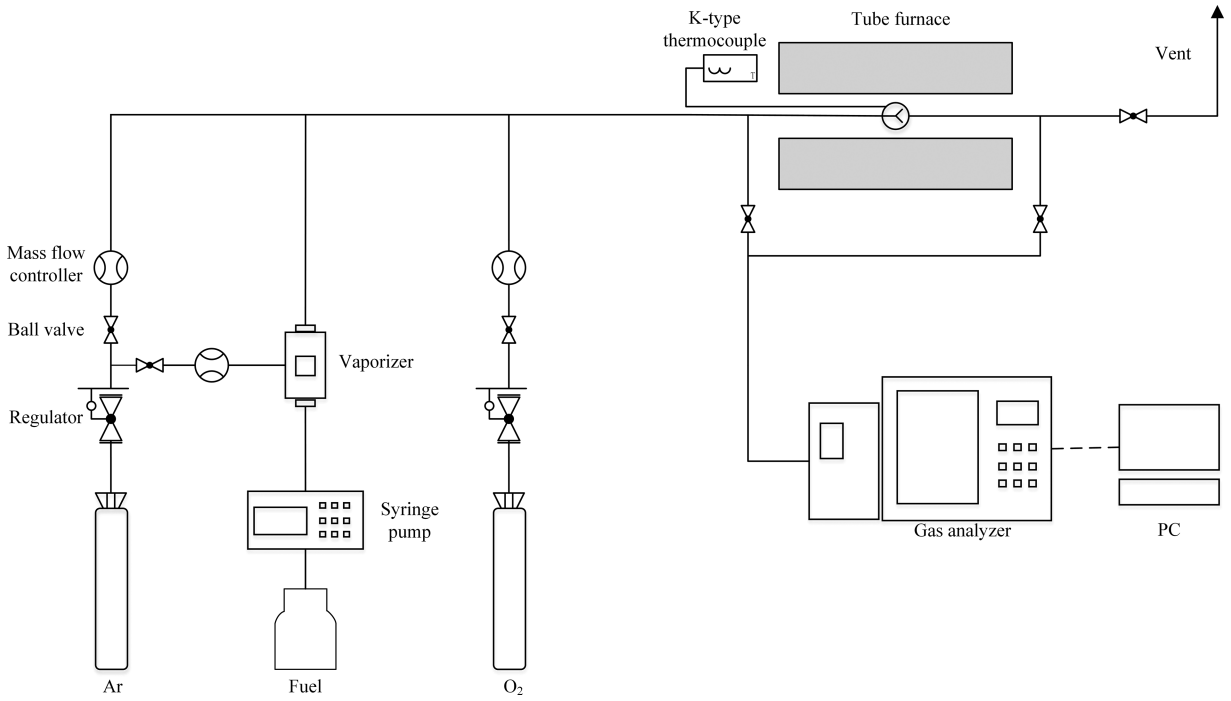

Figure 11. Schematic diagram of the JSR experimental apparatus.

temperature, pressure, and equivalence ratio. The comparisons between the simulation results and measured data indicate that the final mechanism shows good agreement with the experimental data. Therefore, the combination of the reduction method and the genetic algorithm can be effectively applied to the reduction mechanism. The reduced mechanism developed in this study can accurately predict the experimental results, which can be further applied to the simulation of combustion behaviors of *n*-pentanol in internal combustion engines.

5. EXPERIMENTAL SECTION

The main purpose of the current investigation is to establish a reduced mechanism of *n*-pentanol by numerical simulation method, which can be reliably used to analyze the influence of main intermediates and free radicals on the oxidation process and the main generation path of *n*-pentanol. For proving the established models and simulation results, medium- and low-temperature oxidation experiments for *n*-pentanol were performed in the JSR experimental setup at atmospheric pressure. The schematic diagram of the JSR apparatus is shown in Figure 11. The JSR made of fused silica consists of a 58 mm diameter sphere equipped with four nozzles of 1 mm internal diameter and an external quartz tube with a diameter of 6 mm. The design of JSR satisfies the construction rules proposed by Villermaux et al.[29] The JSR was heated in an electrical furnace and the temperature was kept constant using the temperature program heating method. The test temperature was measured by a K-type thermocouple deployed in the center of the reactor. A liquid injection pump was used to supply the liquid fuel to the vaporization tank maintained at 200 °C. The vaporized fuel was diluted by high-purity (99.999%) nitrogen with a high dilution (0.1% fuel volume) and fed into the JSR after mixed with high-purity (99.999%) oxygen. All of the lines before and after the reactor were heated to 200 °C to prevent vaporized fuel liquidation. The JSR may form the homogenous mixture so that the gas components in each part of the reactor are the same and evenly distributed, while the highly diluted fuel reduces the temperature gradient and heat release in the JSR. Gas compositions and flow rate were precisely controlled and metered by mass flow controllers, in which different equivalence ratios according to the test requirements could be prepared. Reaction products were analyzed using GC-MS equipped with capillary columns (DB-wax UI and HP-PLOT Al_2O_3) for hydrocarbons and oxygenated compounds and a thermal conductivity detector for light species such as O_2, CO, CO_2, and H_2.

The experiments were performed with a constant residence time maintained at 2.0 s, over a temperature range from 700 to 1100 K, and equivalence ratios of 0.5, 1.0, and 2.0. The feed stream was continuously flowing in the reactor during the increase of the gas temperature in the JSR. For acquiring steady data at each recording temperature, the species concentrations were recorded until the flow was completely stable.

AUTHOR INFORMATION

Corresponding Author

Chunhua Zhang − *Key Laboratory of Shaanxi Province for Development and Application of New Transportation Energy, Chang'an University, Xi'an 710064, P. R. China;* orcid.org/0000-0002-0349-390X; Phone: +862982334466; Email: zchzzz@126.com

Authors

Songfeng Li − *Key Laboratory of Shaanxi Province for Development and Application of New Transportation Energy, Chang'an University, Xi'an 710064, P. R. China*

Zheng Jing − *Key Laboratory of Shaanxi Province for Development and Application of New Transportation Energy, Chang'an University, Xi'an 710064, P. R. China*

Yangyang Li − *Key Laboratory of Shaanxi Province for Development and Application of New Transportation Energy, Chang'an University, Xi'an 710064, P. R. China*

https://dx.doi.org/10.1021/acsomega.1c00147
ACS Omega 2021, 6, 6448−6459

Peng Yin − *Key Laboratory of Shaanxi Province for Development and Application of New Transportation Energy, Chang'an University, Xi'an 710064, P. R. China*
Panpan Cai − *Key Laboratory of Shaanxi Province for Development and Application of New Transportation Energy, Chang'an University, Xi'an 710064, P. R. China*
An Lu − *Key Laboratory of Shaanxi Province for Development and Application of New Transportation Energy, Chang'an University, Xi'an 710064, P. R. China*

Complete contact information is available at: https://pubs.acs.org/10.1021/acsomega.1c00147

Notes

The authors declare no competing financial interest.

■ ACKNOWLEDGMENTS

This study was supported by the National Natural Science Foundation of China (51806020) and the Special Fund for Basic Scientific Research of Central Colleges, Chang'an University (300102220512, 300102229502, and 300102229202).

■ NOMENCLATURE

A	pre-exponential factor
E	activation energy
T_{in}	initial temperature
Φ	equivalence ratio

■ ABBREVIATIONS

JSR	jet-stirred reactor
GC	gas chromatography
RMG	reaction mechanism generator
ST	shock tube
RCM	rapid compression machine
CFD	computational fluid dynamics
DREGP	direct relationship graph with error propagation
RPA	reaction pathway analysis
ROP	rate of production
SA	sensitivity analysis
GC-MS	gas chromatography-mass spectrometry
PSR	perfectly stirred reactor
NSGA-II	nondominated sorting genetic algorithm II

■ REFERENCES

(1) Vinod Babu, M.; Madhu Murthy, K.; Amba Prasad Rao, G. Butanol and pentanol: The promising biofuels for CI engines − A review. *Renewable Sustainable Energy Rev.* **2017**, *78*, 1068−1088.
(2) Gorbatenko, I.; Tomlin, A. S.; Lawes, M.; Cracknell, R. F. Experimental and modelling study of the impacts of n-butanol blending on the auto-ignition behaviour of gasoline and its surrogate at low temperatures. *Proc. Combust. Inst.* **2019**, *37*, 501−509.
(3) Hinton, N.; Stone, R.; Cracknell, R.; Olm, C. Aqueous ethanol laminar burning velocity measurements using constant volume bomb methods. *Fuel* **2018**, *214*, 127−134.
(4) Çelebi, Y.; Aydın, H. An overview on the light alcohol fuels in diesel engines. *Fuel* **2019**, *236*, 890−911.
(5) Fan, Q. H.; Qi, Y. L.; Wang, Y. D.; Wang, Z. Investigation into pressure dependence of flame speed for fuels with low and high octane sensitivity through blending ethanol. *Combust. Flame* **2020**, *212*, 252−269.
(6) Cancino, L. R.; Fikri, M.; Oliveira, A. A. M.; Schulz, C. Measurement and Chemical Kinetics Modeling of Shock-Induced Ignition of Ethanol−Air Mixtures. *Energy Fuels* **2010**, *24*, 2830−2840.
(7) Heufer, K. A.; Olivier, H. Determination of ignition delay times of different hydrocarbons in a new high pressure shock tube. *Shock Waves* **2010**, *20*, 307−316.
(8) Salvato, L.; Viggiano, A.; Valorani, M.; Magi, V. On the simplification of kinetic reaction mechanisms of air-ethanol under high pressure conditions. *Fuel* **2013**, *104*, 488−499.
(9) Kohse-Höinghaus, K.; Osswald, P.; Cool, T. A.; Kasper, T.; Hansen, N.; Qi, F.; Westbrook, C. K.; Westmoreland, P. R. Biofuel combustion chemistry: from ethanol to biodiesel. *Angew. Chem., Int. Ed.* **2010**, *49*, 3572−3597.
(10) Dagaut, P.; Sarathy, S. M.; Thomson, M. J. A chemical kinetic study of n-butanol oxidation at elevated pressure in a jet stirred reactor. *Proc. Combust. Inst.* **2009**, *32*, 229−237.
(11) Sarathy, S. M.; Thomson, M. J.; Togbé, C.; Dagaut, P.; Halter, F.; Mounaim-Rousselle, C. An experimental and kinetic modeling study of n-butanol combustion. *Combust. Flame* **2009**, *156*, 852−864.
(12) Harper, M. R.; Van Geem, K. M.; Pyl, S. P.; Marin, G. B.; Green, W. H. Comprehensive reaction mechanism for n-butanol pyrolysis and combustion. *Combust. Flame* **2011**, *158*, 16−41.
(13) Zhang, J. X.; Wei, L. J.; Man, X. J.; Jiang, X.; Zhang, Y. J.; Hu, E. J.; Huang, Z. H. Experimental and Modeling Study of n-Butanol Oxidation at High Temperature. *Energy Fuels* **2012**, *26*, 3368−3380.
(14) Heufer, K. A.; Sarathy, S. M.; Curran, H. J.; Davis, A. C.; Westbrook, C. K.; Pitz, W. J. Detailed Kinetic Modeling Study of *n*-Pentanol Oxidation. *Energy Fuels* **2012**, *26*, 6678−6685.
(15) Togbé, C.; Halter, F.; Foucher, F.; Mounaim-Rousselle, C.; Dagaut, P. Experimental and detailed kinetic modeling study of 1-pentanol oxidation in a JSR and combustion in a bomb. *Proc. Combust. Inst.* **2011**, *33*, 367−374.
(16) Wang, G.; Yuan, W. H.; Li, Y. Y.; Zhao, L.; Qi, F. Experimental and kinetic modeling study of n-pentanol pyrolysis and combustion. *Combust. Flame* **2015**, *162*, 3277−3287.
(17) Dayma, G.; Togbé, C.; Dagaut, P. Experimental and Detailed Kinetic Modeling Study of Isoamyl Alcohol (Isopentanol) Oxidation in a Jet-Stirred Reactor at Elevated Pressure. *Energy Fuels* **2011**, *25*, 4986−4998.
(18) Tsujimura, T.; Pitz, W. J.; Gillespie, F.; Curran, H. J.; Weber, B. W.; Zhang, Y.; Sung, C. J. Development of Isopentanol Reaction Mechanism Reproducing Autoignition Character at High and Low Temperatures. *Energy Fuels* **2012**, *26*, 4871−4886.
(19) Sarathy, S. M.; Park, S.; Weber, B. W.; Wang, W.; Veloo, P. S.; Davis, A. C.; Togbe, C.; Westbrook, C. K.; Park, O.; Dayma, G.; Luo, Z.; Oehlschlaeger, M. A.; Egolfopoulos, F. N.; Lu, T.; Pitz, W. J.; Sung, C.-J.; Dagaut, P. A comprehensive experimental and modeling study of iso-pentanol combustion. *Combust. Flame* **2013**, *160*, 2712−2728.
(20) Li, Q. Q.; Tang, C. L.; Cheng, Y.; Guan, L.; Huang, Z. H. Laminar Flame Speeds and Kinetic Modeling of n-Pentanol and Its Isomers. *Energy Fuels* **2015**, *29*, 5334−5348.
(21) Reitz, R. D. Directions in internal combustion engine research. *Combust. Flame* **2013**, *160*, 1−8.
(22) Feng, H. Q.; Zhang, J.; Liu, D. J.; An, M.; Zhang, W. W.; Zhang, X. D. Development of a reduced n-butanol mechanism with combined reduction methods. *Fuel* **2017**, *187*, 403−416.
(23) Díaz-González, M.; Treviño, C.; Prince, J. C. A Reduced Kinetic Mechanism for the Combustion of n-Butanol. *Energy Fuels* **2018**, *32*, 867−874.
(24) Liu, X. L.; Wang, H.; Zheng, Z. Q.; Liu, J. L.; Reitz, R. D.; Yao, M. F. Development of a combined reduced primary reference fuel-alcohols (methanol/ethanol/propanols/butanols/n-pentanol) mechanism for engine applications. *Energy* **2016**, *114*, 542−558.
(25) Chang, Y. C.; Jia, M.; Niu, B.; Xu, Z.; Liu, Z.; Li, Y. P.; Xie, M. Z. Construction of a skeletal oxidation mechanism of n-pentanol by integrating decoupling methodology, genetic algorithm, and uncertainty quantification. *Combust. Flame* **2018**, *194*, 15−27.
(26) Rawadieh, S. E.; Altarawneh, I. S.; Batiha, M. A.; Al-Makhadmeh, L. A.; Almatarneh, M. H.; Altarawneh, M. Reaction of hydroperoxy radicals with primary C_{1-5} alcohols: a profound effect on ignition delay times. *Energy Fuels* **2019**, *33*, 11781−11794.

(27) Heufer, K. A.; Bugler, J.; Curran, H. J. A comparison of longer alkane and alcohol ignition including new experimental results for n-pentanol and n-hexanol. *Proc. Combust. Inst.* **2013**, *34*, 511−518.
(28) Nativel, D.; Pelucchi, M.; Frassoldati, A.; Comandini, A.; Cuoci, A.; Ranzi, E.; Chaumeix, N.; Faravelli, T. Laminar flame speeds of pentanol isomers: An experimental and modeling study. *Combust. Flame* **2016**, *166*, 1−18.
(29) Matras, D.; Villermaux, J. Un réacteur continu parfaitement agité par jets gazeux pour l'étude cinétique de réactions chimiques rapides. *Chem. Eng. Sci.* **1973**, *28*, 129−137.

https://dx.doi.org/10.1021/acsomega.1c00147
ACS Omega 2021, 6, 6448−6459